AGU PUBLICATIONS

Geophysical Research Letters

RESEARCH LETTER
10.1002/2016GL069219

Key Points:
- The total nonlinear signal is strongly influenced by crack orientation
- P/S wave interactions open up the possibility of better imaging of cracks
- Imaging the nonlinear interaction of waves can be done with propagating waves, not just in resonance

Correspondence to:
A. E. Malcolm,
amalcolm@mun.ca

Citation:
TenCate, J. A., A. E. Malcolm, X. Feng, and M. C. Fehler (2016), The effect of crack orientation on the nonlinear interaction of a *P* wave with an *S* wave, *Geophys. Res. Lett.*, *43*, 6146–6152, doi:10.1002/2016GL069219.

Received 18 APR 2016
Accepted 29 MAY 2016
Accepted article online 6 JUN 2016
Published online 20 JUN 2016

The effect of crack orientation on the nonlinear interaction of a *P* wave with an *S* wave

J. A. TenCate[1], A. E. Malcolm[2], X. Feng[3,4], and M. C. Fehler[3]

[1]Geophysics Group, Earth and Environmental Sciences Division, Los Alamos National Lab, Los Alamos, New Mexico, USA, [2]Earth Sciences Department, Memorial University of Newfoundland, St. John's, Newfoundland and Labrador, Canada, [3]Department of Earth, Atmospheric, and Planetary Sciences, Massachusetts Institute of Technology, Cambridge, Massachusetts, USA, [4]College of Geo-Exploration Science and Technology, Jilin University, Changchun, China

Abstract Cracks, joints, fluids, and other pore-scale structures have long been hypothesized to be the cause of the large elastic nonlinearity observed in rocks. It is difficult to definitively say which pore-scale features are most important, however, because of the difficulty in isolating the source of the nonlinear interaction. In this work, we focus on the influence of cracks on the recorded nonlinear signal and in particular on how the orientation of microcracks changes the strength of the nonlinear interaction. We do this by studying the effect of orientation on the measurements in a rock with anisotropy correlated with the presence and alignment of microcracks. We measure the nonlinear response via the traveltime delay induced in a low-amplitude *P* wave probe by a high-amplitude *S* wave pump. We find evidence that crack orientation has a significant effect on the nonlinear signal.

1. Introduction

Rocks, especially sedimentary rocks, are peculiar materials. This is particularly apparent when attempting to describe the exceedingly large nonlinear behavior seen in rocks. The physical origin for much of this nonlinearity has often been ascribed to (sticky) cracks [e.g., *Pecorari*, 2003]. By sticky cracks, we mean cracks that respond slowly to changes in stress or strain (i.e., they stick), and their response is not symmetric with respect to increasing and decreasing stress. That cracks have a large impact on wave velocities in rocks is well known, and it is the closing of those cracks that causes changes in velocity with pressure [*Gardner et al.*, 1974; *Gist*, 1994]. It is thus reasonable to postulate that cracks play a large role in the observed strong nonlinearity of rocks [*Guyer and Johnson*, 2009] and other materials [*Van Den Abeele et al.*, 2009], but there are few truly definitive experiments that explore the role of microcracks and their orientations on nonlinear elasticity. The research described here begins to provide such evidence.

Understanding the data that we observe requires the use of aspects of the theory of nonlinear wave propagation in fluids as well as in solids. Nonlinearity in fluids is easy to understand, and the physics is well established [*Hamilton and Blackstock*, 1997]. While the nonlinear physics in ordinary solids is complicated, it is also known [*Landau and Lifshitz*, 1970]. Although at first glance one would expect nonlinear wave propagation in rocks to more closely resemble that in a solid, in fact, the equations chosen to describe the nonlinear wave propagation in rocks resemble those in fluids with strain taking the place of particle velocity [e.g., *TenCate et al.*, 1996]. For example, a wave passing through a fluid sets the fluid in motion (convection), similarly a wave passing through a rock containing cracks and fluids, may set the fluid in motion. We use these ideas to explain, at least qualitatively, our observed results.

2. Background

The nonlinear interaction of two acoustic waves in a fluid (e.g., air or water) was a topic of great interest in the 1970s, driven by research in sonic booms and underwater imaging. One set of experiments is of particular note here, the modulation of sound by sound [e.g., *Zverev and Kalachev*, 1970]. These experiments were designed to study the effect that a large-amplitude, low-frequency *P* wave (the pump) had on a weak, high-frequency *P* wave (the probe) when both are traveling in the same direction. The high-amplitude *P* wave pump not only altered the sound speed of the fluid but also set the fluid in motion; as it propagated the pump waveform

started to distort and form a shock. This distorting pump then modulated the small *P* wave probe traveling with it in an understandable way.

Modern variations of these early experiments have been used in biological fluids to characterize the nonlinearity of tissue [*Ichida et al.*, 1983]. In solids, the nonlinear interaction of two waves was described some time ago by *Gol'dberg* [1960]. More recently, *Renaud et al.* [2009, 2011, 2012] have done experiments in nondestructive testing where a small probe wave is affected by a standing wave in a method they call dynamic acoustoelasticity testing (DAET). DAET techniques have also been used in solids to examine materials ranging from bone to concretes to rocks [*Rivière et al.*, 2013]. As detailed in the following section, DAET is a notably different method than the one we use. DAET sets up a steady state resonance in the sample and measures time delays of a high-frequency probe wave that travels through different parts of the resonance wave field. Here we perform a simpler experiment and concentrate on the propagation delays of a high-frequency probe wave caused by the passage of a few cycles of a low-frequency pump wave. This allows us to study the development of the nonlinear response in a transient signal rather than in a steady state as done in DAET. In addition, unlike previous experiments, our low-frequency pump wave is a shear wave, propagating orthogonal to the *P* wave probe, with particle motion aligned with that of the *P* wave. Initial research by *Gallot et al.* [2015] describes the viability of the method and gives results for a homogeneous isotropic Berea sandstone. The research reported here is the first to make use of the method described in *Gallot et al.* [2015] to explore an anisotropic sandstone with an interesting and known texture [*Benson et al.*, 2005], and the results show that we can begin to identify specific mechanisms for the large nonlinearity seen in similar rocks.

3. Experiment

A rectangular slab (15 cm × 15 cm × 5 cm) of Crab Orchard sandstone was chosen for these experiments (Crab Orchard, TN, Kocurek Industries, TX). In contrast to the initial study using Berea sandstone [*Gallot et al.*, 2015], Crab Orchard sandstone (COS) exhibits a very well-characterized anisotropy which has been extensively studied and is reported on by *Benson et al.* [2005]. They showed that both the elastic and flow anisotropy in COS decrease under confining pressure; this along with other measurements they report indicate that the anisotropy is primarily due to fractures that are preferentially aligned parallel to the bedding planes. We begin with a sample with bedding planes normal to the 15 cm × 15 cm face. Measured sound speeds of the sample used in the current experiments, in both directions, very nearly match those of the samples described, measured, and characterized by *Benson et al.* [2005]. Thus, we presume that the analysis and description of the fabric of their samples applies to our sample as well, in other words we assume that the rock has a microstructure dominated by aligned cracks.

As in *Gallot et al.* [2015], a slab of COS was placed standing upright on one of its 5 cm × 15 cm faces. The *S* wave pump was transmitted with a low-frequency 0.1 MHz/1.0″ Olympus/Panametrics V1548 *S* wave transducer mounted (using honey as a couplant) at the top center of the slab, broadcasting downward. The shear wave pump was polarized either in the direction of the bedding planes or—depending on slab rotation—perpendicular to them, as depicted in Figure 1. (The particle motion of the pump is aligned with that of the probe in all experiments.) A pair of high-frequency transmit/receive Olympus/Panametrics *P* wave transducers (1.0 MHz/0.5″ V103) were mounted to both sides of the slab (designated "*P* wave probe" and "receiver"). The probe geometry was such that a short, 1 cycle, *P* wave pulse could be timed so that it traveled through various phases (e.g., a peak or trough) of the passing low-frequency shear wave pump. As seen already in Berea sandstone, the expected effect is a change in the propagation speed of the probe due to the passage of the pump. More specifically, the pump slows the probe down; this slowdown is larger as the probe travels through a trough of the pump and smaller as the probe travels through a peak of the pump, resulting in a clear signature of the pump frequency on the probe traveltime. In both orientations of the sample, the two waves interact in roughly the same region of the rock, minimizing the impact of rock heterogeneities on our measurements.

At the region of interaction of pump and probe waves we pointed a Polytec CLV 3-D laser vibrometer on the surface to accurately measure—and thus control and set—the amplitude of the passing shear wave. The amplitude and shape of this recorded particle velocity were very similar between the two experiments; the normalized L_2 difference between the envelopes of the two laser signals is 15%, and the normalized difference in their maximum amplitudes is less than 2%. The peak strain of the pumps were on the order of a microstrain, as discussed below. A movie of the wavefield produced by the shear wave source in the slab was

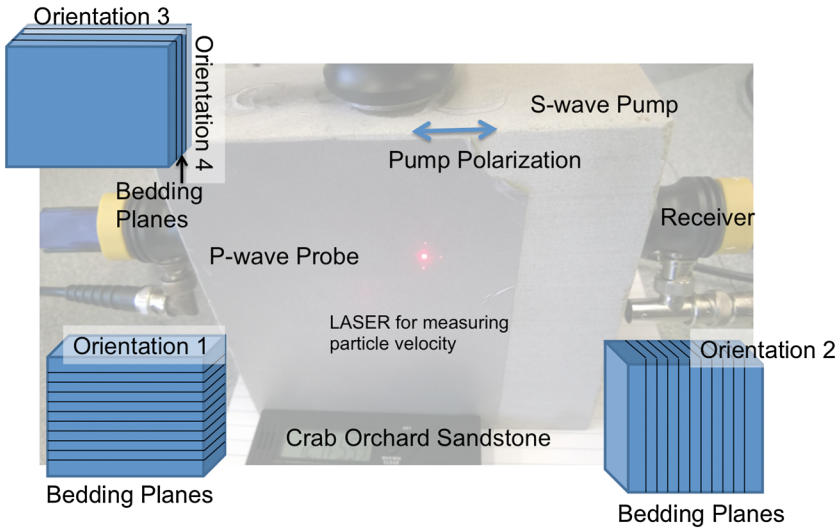

Figure 1. Experimental setup, including the definition of the two orientations of the sample, as used in Figure 3.

made by scanning the surface with the laser vibrometer; this signal was also modeled numerically. The agreement between model and measurement were good [*Gallot et al.*, 2014]. Both measurements and modeling show that shear wavefronts directly beneath the *S* wave transducer are nearly planar and well collimated, and the particle velocity in the shear wave source polarization direction is by far the largest.

The probe and pump wave pulses were produced by an Agilent Dual Function/Arbitrary Waveform Generator synced to fire the *P* wave probe and *S* wave pump tone bursts simultaneously. In addition, the timing of the probe could be successively delayed from shot to shot to vary the portion of the passing shear wave pump wavefield that the probe interacts with. The shear wave pump signal from the generator was amplified with an E&I 240L RF power amplifier (fixed gain) and sent to the transducer; no amplifier was used for the probe transmit transducer. Both pump and probe waveforms were recorded by a *P* wave transducer directly opposite the probe source, on a digital storage oscilloscope always sampling at greater than or equal to 250 Ms/s. As the oscilloscope has limited dynamic range, a Krohn-Hite filter was used to suppress the overwhelmingly large signal from the pump on the probe receiver. As mentioned above, peak strains were measured and held constant throughout all of the experiments and were on the order of 1 microstrain for the pump, and 2 orders of magnitude smaller for the probe. Pump frequency was set to 74 kHz and probe frequency at 620 kHz. Both frequencies were chosen because they were "sweet spots," where each transducer was found to input the maximum amplitude signal with minimum ringing into the sample, (resulting in pure, unambiguous signals). Finally, the two pulses were short enough and the sample large enough that no echoes or wall reflections interfered with the signals of interest. After a suitable wait time for the pulses to die away (2–10 ms), the pump and probe could be fired again. Averaging was used to increase signal to noise ratios. As mentioned above, this experiment follows that of *Gallot et al.* [2015]; the details we have mentioned here are those that are specific to our experiment. The same sample was reoriented to collect data in two directions relative to the orientation of the aligned cracks to highlight the impact these aligned structures have on the nonlinear signal (orientations 1 and 2 in Figure 1). Measurements are made on the center of the sample so that the pump and probe interact in the same region of the sample in both orientations.

4. Results

Figure 2 shows a series of *P* wave probe propagation delay times as a function of the time where the probe first begins to interact with the shear wave. The probe is propagating in the slow direction across the rock sample, i.e., perpendicular to the crack faces. The pump is propagating parallel to the crack faces (orientation 2) with particle motion in the direction of the probe propagation. The solid line is simply the data low-pass filtered and is shown to guide the eye. Processing details are elaborated by *Gallot et al.* [2015] and are also similar to techniques used in DAET. Plotted are the probe time delay relative to the time it takes for the probe to cross the sample when the pump is turned off. The horizontal axis shows the phase delay between the pump and probe offsets at their respective transducers. Zero microseconds on the *x* axis corresponds roughly to the arrival of

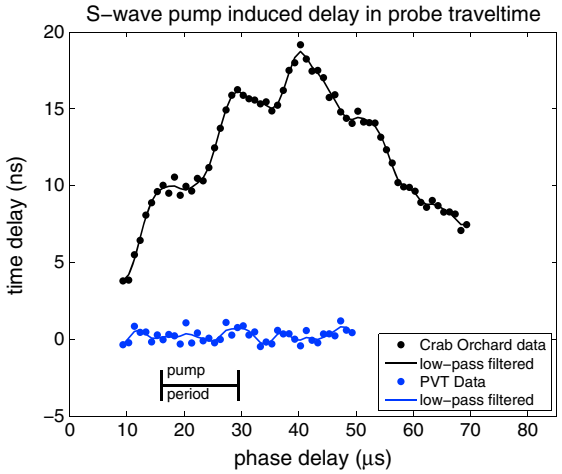

Figure 2. Measured time delay induced in the *P* wave probe by the passage of the *S* wave pump in the Crab Orchard sandstone (block 1, orientation 2) sample and a linear control. The time delay has two distinct frequency bands; the low-frequency signal has the approximate shape of the pump envelope and the high-frequency (ripples) signal is at the frequency of the *S* wave pump. The blue data set was collected in a known linear sample (polyvinyl toluene (PVT)) and shows virtually no delay indicating that our experimental setup is indeed measuring the nonlinearity of the rock sample. Zero microseconds on the *x* axis corresponds roughly to the arrival time of the shear pump at the interaction region.

the shear wave pulse at the interaction point; in this case there is no propagation delay in the probe traveltime across the sample. Two effects are readily apparent in the data shown in the figure. First there is a dominant overall time delay curve, the shape of which matches the shape of the envelope of the actual transmitted shear wave pulse emitted from the transducer into the sample (as measured with the laser vibrometer). This signal is present because it takes some time for the rock to return to equilibrium (this is slow dynamics [*Ten Cate and Shankland*, 1996]), and this time is longer than the period of the pump. This time is related to the energy input into the system, and as a result, we see an imprint of the energy input into the sample, i.e., the envelope of the pump signal. Because this signal tracks the envelope of the pump, with only a small delay, we can conclude that the 2–10 ms wait time between successive data points is sufficient (being 40–200 times the length of the four-period pump signal). The second signal we see is the higher-frequency "ripples" superimposed on top of the overall amplitude envelope. These sinusoidal ripples match the period of the shear wave pump (13.5 μs); there are speed ups where the probe travels primarily through a peak of the shear wave pump and slow downs where the probe travels primarily through a trough. This occurs because the shear wave peaks slightly harden the rock while the troughs slightly soften it. To rule out any nonlinearities in the experiment or processing, a plastic slab of similar mechanical impedance ($Z = \rho c$), and size was substituted for the rock. That result is plotted in blue in Figure 2 for reference. As expected, within the estimated error of the experiment (roughly ±1 ns), no propagation time delays nor an envelope nor ripples were observed with the plastic standard using the same input shear wave amplitude and the same experimental setup.

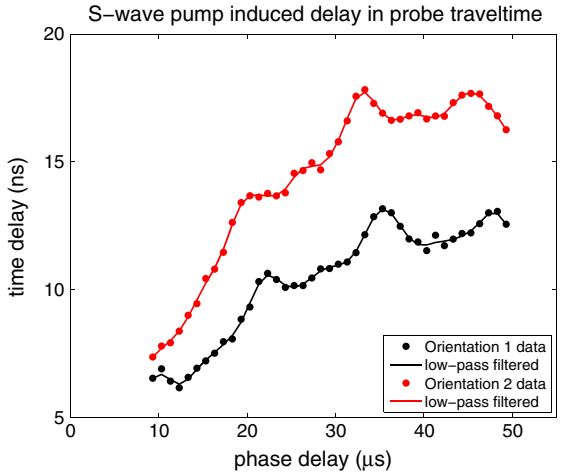

Figure 3. Experimental data as a function of the sample orientation and thus that of the cracks. The red data set is taken with the *S* wave pump particle motion parallel to the bedding planes and shows a much stronger signal than that taken when the pump particle motion is perpendicular to the bedding planes, shown in black. Errors are approximately ±1 ns, determined by repeatability tests and the magnitude of the signal observed in PVT in Figure 2. The two signals were recorded with the same source amplitude; the normalized L_2 difference between the envelopes of the two pump signals is 15%; the normalized difference in their maximum amplitudes is less than 2%.

To determine the effect of fracture orientation on the nonlinear signal, we plot in Figure 3 data in the same sample taken with two orientations: one with the bedding planes parallel (orientation 1) and one perpendicular (orientation 2) to the propagation direction of the shear wave. Care was taken, so the input shear wave amplitudes were the same in both experiments and that this resulted in signals that had the same amplitude at the start

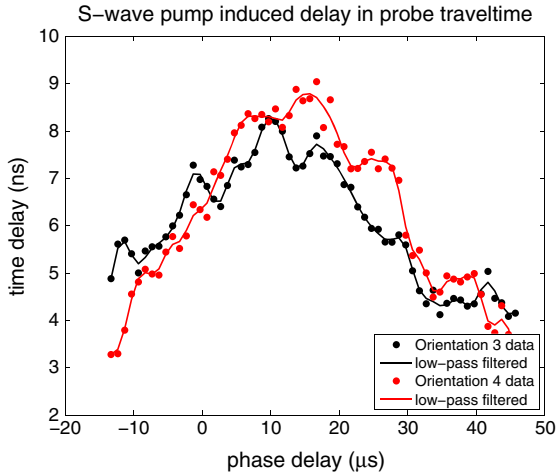

Figure 4. Experimental data as a function of the sample orientation for block 2, where the bedding planes are parallel to the pump particle motion in both orientations. In this case, we see little change in the signal with orientation. Errors are approximately ±1 ns, determined by repeatability tests and the magnitude of the signal observed in PVT in Figure 2. The two signals were recorded with the same source amplitude; the normalized L_2 difference between the envelopes of the two pump signals recorded on an *S* wave transducer on the face opposite the pump transducer is 30%; the normalized difference in their maximum amplitudes is also 30%.

of the interaction region; the data sets were also collected sequentially to minimize variations in room conditions. The data sets shown here were completed within an hour of one another, with a few minutes in between the collection of the two data sets to reset the experiment in the new orientation. The wait time between collecting data points within a single data set was 2–10 ms, which is much longer than the length of the pump wave and its reverberations. As can be seen from Figure 3, when the bedding planes are perpendicular to the shear wave particle motion (orientation 2), the overall time delay is greater than when the shear wave particle motion is parallel to the bedding planes (orientation 1). We observe that the propagation delays (and hence the nonlinearity) depend on orientation. From the observations of *Benson et al.* [2005], we know that the crack faces are predominately parallel to the bedding planes, which indicates that we are observing a much larger effect when the particle motion of both the pump and probe are perpendicular to the crack faces. We then repeated the experiment in a different lab with similar equipment, on a different sample cut with the bedding planes parallel to the large face, as shown in Figure 1; the results of this experiment are shown in Figure 4. For these data, we see little or no dependence on the sample orientation. This is expected since we are not changing the orientation of the cracks relative to the particle motion of the pump and probe in this case and supports our hypothesis that it is the crack orientation that is causing the difference observed in Figure 3.

5. Comparison and Discussion

Although there are no other experiments we know of that definitively compare the effect of crack orientation on nonlinear wave interaction, comparison with other nonlinear acoustoelastic measurements are possible. Note that the maximum traveltime delay observed in the data of Figure 3 is roughly 20 ns; the amplitude of the high-frequency traveltime oscillations superimposed on that overall envelope is approximately 5 ns. In these experiments, with a total travel time across the sample of approximately 48 μs, the maximum induced velocity change due to the passage of the shear wave pump is 0.04%, and the additional high-frequency variations correspond to a velocity change of about 0.01%.

To estimate the strain induced by the shear wave pump, we measured the particle velocity as a function of time and position across the central part of the sample (including the pump/probe interaction region), with a Polytec 3-D laser vibrometer. These measurements indicate that the shear *S* wave particle motion is dominant in the interaction region, so we have ignored any *P* waves generated from the outer edge of the transducer. At a fixed point in the center of the interaction region, the measured shear wave particle velocity is 1.6 mm/s which corresponds to an approximate strain of 8×10^{-7}. (This strain is estimated by dividing the measured particle velocity by the phase velocity; this gives precisely the strain for a plane wave.) At that strain, the high-frequency traveltime delays measured here are in general agreement with those published in recent dynamic acoustoelasticity testing results (DAET) described by *Renaud et al.* [2012] and others even though our pump is a shear wave while the DAET experiments used a *P* wave pump.

In addition, assuming that the above strain value is e_{xz} (where *z* is the direction of pump wave propagation and *x* is the direction of particle motion), we use a linear Hooke's Law to compute an estimated stress of 6.5 kPa

induced by the shear wave pump. In contrast, *Winkler and McGowan* [2004] examined the change in *P* and *S* wave velocities as a function of quasi-static stress between 0 and 6 MPa (see their Figure A1), larger by 3 orders of magnitude than the stresses observed in our experiment. Their measurements show a change in *P* wave velocity of approximately 7% under uniaxial stress for a dry Berea sandstone. A simple extrapolation suggests that we should expect to see roughly 1/1000th of the velocity change in our experiments compared to those seen by Winkler and McGowan (i.e., we would expect to see a 0.007% change in velocity). Instead, there is much more; the *S* wave pump has induced a velocity change about 50 times larger (at 0.04%) than might be expected from the quasi-static acoustoelasticity measurements. It is possible that the physics seen in our experiment differs significantly from the quasi-static results because of higher frequencies or perhaps using a shear wave as a pump activates a different form of nonlinearity in the rock. It is not uncommon to see differences like this; e.g., values of nonlinearity found from quasi-static measurements versus those from dynamic measurements are often not the same [see, e.g., *D'Angelo et al.*, 2008].

There are several physical phenomena highlighted by this experiment. The high-frequency ripples seen in the measured time delays have the same frequency as the pump showing that the probe wave is speeding up or slowing down in response to the passage of the shear wave pump. This is something one would expect to see in a fluid, with *P* wave excitation, but it is not clear what the cause of this effect is in a cracked solid. It could be associated with a change in length of the sample, but the required strains to cause the necessary change in length are 10^{-4}, which is larger than our estimated strain of 10^{-6}. In addition, as already mentioned, similar experiments with an intact slab of plastic showed no such time delays suggesting that a change of length is unlikely to be the cause of the ripples.

Another possible source of the signature and shape seen in the data here could be the opening and closing of cracks in the solid. As mentioned above, *Benson et al.* [2005] found that the Crab Orchard Sandstone has cracks that are primarily aligned with the bedding planes; thus, we designed our experiment to highlight the influence of these cracks. However, while the amplitude of the low-frequency envelope is different for the two sample orientations (with a difference of 4.5 ns in maximum time delay), the high-frequency oscillations change less with sample orientation (with both data sets having a ripple amplitude of 1.7 ns), indicating that crack opening and closing is likely not the main cause of the observed high-frequency ripples. This does not diminish the effect that cracks have on the signal but does make it rather more difficult to explain. Investigations into the role of grain-grain and cement-grain interactions may help to resolve this issue.

Finally, it's also clear from experiments done over several months that room conditions, notably room humidity, have an important effect on the observed ripples. This suggests that the high-frequency oscillations driven by the shear wave pump frequency are influenced by changes in the pore structure of the rocks and specifically from changes in humidity in an important way. The effects of room conditions, especially relative humidity, on nonlinear measurements like these is the subject of a forthcoming publication.

6. Conclusions

We have reported on experiments done to determine the effect of crack orientation on the nonlinear time delays recorded in a dynamic nonlinear elasticity experiment. Our experiment examined the effect of crack orientation on the delay times in a *P* wave probe, caused by the passage of an *S* wave pump wave. We have confirmed, as shown in other experiments, that the resulting signal has two frequencies, one at the frequency of the *S* wave pump (ripples) and another at a much lower frequency. We do not observe significant changes in the former signal associated with crack orientation, but we do see significant change in the latter, low-frequency signal. Although we are not able to pin down the precise physical mechanism underlying the results seen here, we have presented strong evidence that the nonlinear signal is strongly dependent on crack orientation, representing a first step toward imaging crack orientation remotely.

Acknowledgments
We are grateful to the funding received for this work from the following: Weatherford (J.T., A.M., and M.F.), the National Natural Science Foundation of China under grant 41430322 (X.F.), Chevron (A.M.), the Natural Sciences and Engineering Research Council of Canada (A.M.), Research and Development Corporation of Newfoundland and Labrador (A.M.), and the Hibernia Development and Management Corporation (A.M.). We also thank Ingo Geldmacher and John Hallman of Weatherford and Dan Burns, Steve Brown of MIT, and Thomas Gallot of Universidad de la Republica, Uruguay, for useful discussions. Data from this work can be obtained by emailing the authors.

References

Benson, P., P. Meredith, E. Platzman, and R. White (2005), Pore fabric shape anisotropy in porous sandstones and its relation to elastic wave velocity and permeability anisotropy under hydrostatic pressure, *Int. J. Rock Mech. Mining Sci.*, *42*(7–8), 890–899, doi:10.1016/j.ijrmms.2005.05.003.

D'Angelo, R. M., K. W. Winkler, and D. L. Johnson (2008), Three wave mixing test of hyperelasticity in highly nonlinear solids: Sedimentary rocks, *J. Acoust. Soc. Am.*, *123*(2), 622–39, doi:10.1121/1.2821968.

Gallot, T., A. Malcolm, D. Burns, S. Brown, M. Fehler, and T. Szabo (2014), *Nonlinear Interaction of Seismic Waves in the Lab: A Potential Tool for Characterizing Pore Structure and Fluids*, Soc. of Exploration Geophys., Denver, Colo.

Gallot, T., A. Malcolm, T. Szabo, S. Brown, D. Burns, and M. Fehler (2015), Characterizing the nonlinear interaction of *S*- and *P*-waves in a rock sample, *J. Appl. Phys.*, *117*, 34902.
Gardner, G., L. Gardner, and A. Gregory (1974), Formation velocity and density-the diagnostic basics for stratigraphic traps, *Geophysics*, *39*(6), 770–780.
Gist, G. (1994), Fluid effects on velocity and attenuation in sandstones, *J. Acoust. Soc. Am.*, *96*(2), 1158–1173.
Gol'dberg, Z. (1960), Interaction of plane longitudinal and transverse elastic waves, *Sov. Phys. Acoust*, *6*(3), 307–310.
Guyer, R., and P. Johnson (2009), *Nonlinear Mesoscopic Elasticity*, Wiley-VCH, Weinheim, Germany.
Hamilton, M., and D. Blackstock (1997), *Nonlinear Acoustics*, Academic Press, Melville, N. Y.
Ichida, N., T. Sato, and M. Linzer (1983), Imaging the nonlinear ultrasonic parameter of a medium, *Ultrason. Imaging*, *5*(4), 295–299, doi:10.1177/016173468300500401.
Landau, L., and E. Lifshitz (1970), *Theory of Elasticity*, Pergamon Press, Oxford, U. K.
Pecorari, C. (2003), Nonlinear interaction of plane ultrasonic waves with an interface between rough surfaces in contact, *J. Acoust. Soc. Am.*, *113*(6), 3065, doi:10.1121/1.1570437.
Renaud, G., S. Calle, and M. Defontaine (2009), Remote dynamic acoustoelastic testing: Elastic and dissipative acoustic nonlinearities measured under hydrostatic tension and compression, *Appl. Phys. Lett.*, *94*(1), 11905, doi:10.1063/1.3064137.
Renaud, G., M. Talmant, S. Callé, M. Defontaine, and P. Laugier (2011), Nonlinear elastodynamics in micro-inhomogeneous solids observed by head-wave based dynamic acoustoelastic testing, *J. Acoust. Soc. Am.*, *130*(6), 3583–3589, doi:10.1121/1.3652871.
Renaud, G., P.-Y. Le Bas, and P. A. Johnson (2012), Revealing highly complex elastic nonlinear (anelastic) behavior of Earth materials applying a new probe: Dynamic acoustoelastic testing, *J. Geophys. Res.*, *117*, B06202, doi:10.1029/2011JB009127.
Rivière, J., G. Renaud, R. Guyer, and P. Johnson (2013), Pump and probe waves in dynamic acousto-elasticity: Comprehensive description and comparison with nonlinear elastic theories, *J. Appl. Phys.*, *114*, 54905.
Ten Cate, J., and T. Shankland (1996), Slow dynamics in the nonlinear elastic response of Berea sandstone, *Geophys. Res. Lett.*, *23*(21), 3019–3022.
TenCate, J. A., K. E. A. Van Den Abeele, T. J. Shankland, and P. A. Johnson (1996), Laboratory study of linear and nonlinear elastic pulse propagation in sandstone, *J. Acoust. Soc. Am.*, *100*(3), 1383, doi:10.1121/1.415985.
Van Den Abeele, K., P. Y. Le Bas, B. Van Damme, and T. Katkowski (2009), Quantification of material nonlinearity in relation to microdamage density using nonlinear reverberation spectroscopy: Experimental and theoretical study., *J. Acoust. Soc. Am.*, *126*(3), 963–72, doi:10.1121/1.3184583.
Winkler, K. W., and L. McGowan (2004), Nonlinear acoustoelastic constants of dry and saturated rocks, *J. Geophys. Res.*, *109*, B10204, doi:10.1029/2004JB003262.
Zverev, A., and A. Kalachev (1970), Modulation of sound by sound in the intersection of sound waves, *Sov. Phys. Acoust.*, *16*, 204–208.